J. Fluid Mech. (1976), *vol.* 73, *part* 2, *pp.* 241–264
Printed in Great Britain

Vorticity concentration and the dynamics of unstable free shear layers

By G. M. CORCOS AND F. S. SHERMAN
Department of Mechanical Engineering, University of California, Berkeley

(Received 10 February 1975 and in revised form 1 September 1975)

The detailed dynamics of an unstable free shear layer are examined for a gravitationally stable or neutral fluid. This first article focuses on the part of the evolution that precedes the first subharmonic interaction. This consists of the transformation of selectively amplified sinusoidal waves into periodically spaced regions of vorticity concentration (the cores) joined by thin layers (the braids), in which vorticity is also concentrated. The thin layers are the channels along which vorticity is advected into the cores, and the cores provide the strain which creates the braids. For moderately long waves an analysis is given of the braid structure as a function of time. For gravitationally stable shear layers at high Reynolds numbers, the local vorticity reaches such large values as to cause secondary shear instability on a small (length) and short (time) scale. A physical account of the primary instability and its self-limiting mechanism is used as a basis for a computation, which yields growth rates and maximum amplitude as a function of initial layer parameters. The computation supplies the wavelength of waves that grow to achieve the largest (absolute) amplitude. Finally, the model makes it clear that, in the absence of secondary instability, this initial phase of the nonlinear development of the layer contributes only a modicum of additional mixing, especially at high Reynolds numbers.

1. Introduction

In the problem treated numerically in Patnaik, Sherman & Corcos (1976), the vorticity is originally uniform in x, and distributed within a finite thickness, with a maximum at the centre of the layer. In addition, the region of density change is somewhat thicker than the region of velocity variation, so that the fluid is least stable at the centre of the layer. The computations reveal that, as the wave grows, the following transformation takes place. A narrow region of closed streamlines, the 'cat's eye', introduced with the initial disturbance, widens. With time, an increasing fraction of the total vorticity is found within the expanding recirculating region. This in turn causes an induced strain field to be established along the dividing streamlines between the cats' eyes, and, particularly, near the stagnation points. (See figure 1.) There is a positive strain along one of the dividing streamlines, negative strain along the other. The strain field tends to centre the vorticity and density distributions along a direction with positive strain, and to thin those layers (and consequently intensify density and vorticity gradient

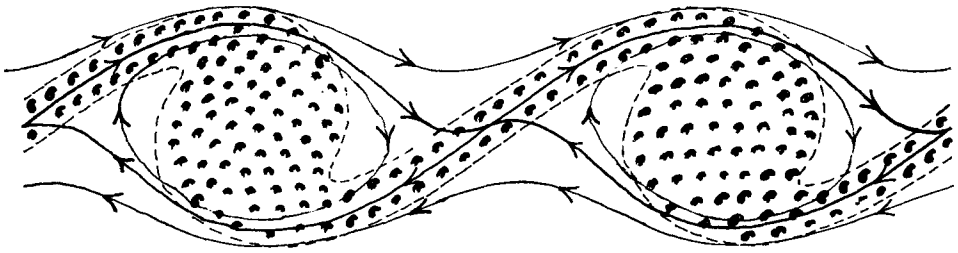

FIGURE 1. Vorticity concentration. ———, streamlines. Vorticity is concentrated within the shaded area. Note the strain field in the centre of the picture.

across them). If the dividing streamline were stationary, the layers thus formed would be aligned with it; but it rotates as the wave grows and the layer rotation near the stagnation point (where this effect is strongest) lags somewhat behind that of the streamline, particularly during the early stages of the growth. Both vorticity and density distributions are thus extruded on both sides of the stagnation point, more or less along the stagnation streamline, towards and apparently through the expanding edge of the cat's eye. The tilted and narrow layer of density gradient (the braid) is strongly baroclinic, and so also a source of vorticity.

It is, of course, of interest to supply an analytic and physical framework for the description of such a process, one that should be suitable to the high Reynolds numbers typical of oceanic and atmospheric shear layers, for which finite grid computations are ill-suited. We shall see that the process described above is the means by which vorticity is redistributed, and that the various stages of the instability of the layer correspond to the modes of horizontal migration of the vorticity from an initial distribution uniform in x.

In what follows, we shall examine first, by simple analytical methods applicable to high Reynolds numbers, the evolution of the flow near the stagnation points. In particular, we shall give estimates of the thickness of both the density and the vorticity layers as a function of time, and consider the possibility of occurrence (in the baroclinic or initially gravitationally stable case) of small-scale or secondary instability in the braids. The analysis applies only after an initial period of growth, and for sufficiently small non-dimensional wavenumbers.

We shall also synthesize the basic features of the nonlinear instability in a model designed to explain why finite waves or billows reach a maximum amplitude, how fast the wave is constrained to grow, and what role a stable or unstable vertical density difference plays in the growth. Our physical account of the instability prepares us to suspect that waves of only slightly different wavelengths cannot grow simultaneously to large amplitude, and to view the phenomenon of vortex pairing, or the dominance of subharmonics, as a qualitatively similar repetition of the initial nonlinear instability, a sort of binomial hierarchy of instabilities which goes on without end in a barotropic shear layer, but which is limited by buoyancy in gravitationally stable cases.

Finally, our model will lead to an estimate of the maximum thickness of a mixing layer which evolves from an initial thermocline or inversion with a given density difference and shear.

Both subharmonic generation (i.e. the stepwise increase in the scale of the instability), and the terminal state of a gravitationally stable layer will be discussed in a subsequent paper.

2. The structure of inner diffusive and viscous layers in the neighbourhood of stagnation points

In order to study the structure of the vorticity and density layers near stagnation points, two assumptions will be made. They are suggested by the numerical results of Patnaik *et al.* (1976), and defended below. The first assumption is that the vorticity and temperature layers are thin, and that the strain along them is analytic around the stagnation point. The second is that, even though the vorticity found in the braid near the stagnation point induces a substantial local velocity, that part of the velocity plays no role in the advection of either temperature or vorticity. In other words, the *local* vorticity can be treated as a passive scalar.

The co-ordinates chosen are locally orthogonal, and centred in the middle of the braid (figure 6). Braid radii of curvature are assumed large next to layer thickness. The origin is the stagnation point. s is the streamwise co-ordinate in the direction along which the vorticity and density gradients are assumed concentrated;† η, a co-ordinate normal to s. The velocity $\mathbf{u}$ has components u (along s) and v (along η).

We wish to distinguish between the velocity $\mathbf{u}_c$, induced by the vorticity broadly distributed within the cat's eyes and the ends of the braids, and the velocity $\mathbf{u}_s$, induced by the vorticity in the thin, inclined braids. Each is assumed to satisfy continuity separately.

The velocity $\mathbf{u}_c$ has, after the braids are formed, characteristic magnitude U (where U is half the initial shear) and characteristic scale λ. Such a scaling follows from the Biot–Savart Law. The component v_c along η vanishes on $\eta = 0$, and elsewhere has order of magnitude $(\eta U/\lambda)$. Call δ the characteristic braid thickness. The velocity induced locally by the concentrated vorticity layer may have order of magnitude U also. If the braids are thin and nearly straight, and if the braid vorticity is nearly uniform with s, component v_s will be negligible.

Thus, if R is the braid radius of curvature, provided $\delta/R \ll 1$ and $\partial\Omega/\partial s \ll \Omega/\lambda$, the dominant components of the velocity in the braid around the stagnation points are

$$u = u_c(s, 0) - \int_0^\eta \Omega \, d\eta, \quad v = -\int_0^\eta \frac{\partial u_c}{\partial s} d\eta.$$

(Ω is the vorticity.) Furthermore, if satisfactory local solutions are found for the vorticity such that $\partial\Omega/\partial s = 0$, then for any scalar A, independent of s, $\mathbf{u}.\nabla A$ reduces to $v_c \partial A/\partial\eta$. We shall assume first, and verify *a posteriori*, that these conditions are satisfied.

† In what follows, we overlook the rotation of the co-ordinate system, which adds a small amount of relative vorticity to the braid. It is easy to show that the error due to this omission is negligible for high Reynolds numbers.

Now, it is found in Patnaik *et al.* (see our figure 7) that, along the braids and to good accuracy over a length typically $\frac{1}{2}\lambda$, $u_c(s, 0) = \gamma(t)\, s$, where γ is independent of s.† Hence, to order δ/λ,

$$u_c(s, \eta) \simeq \gamma s \quad \text{and} \quad \mathbf{u}.\nabla A = -\gamma\eta\, \partial A/\partial\eta.$$

It is possible that solutions derived from the foregoing assumptions become accurate only a certain time after the onset of instability. Moreover, it will be clear from the solutions that they require a minimum Reynolds number to be justified. Such restrictions are similar to those which attend the application of boundary-layer theory to boundaries which have a sharp leading edge, and for which boundary-layer approximations are valid only beyond a minimum distance downstream of the leading edge.

2.1. *Similarity solution for the density*

In the s, η co-ordinate system, and with the 'boundary-layer' approximations just discussed, Patnaik *et al.* (1976, (2.3)) is reduced to

$$\frac{\partial\rho}{\partial t} - \gamma\eta\frac{\partial\rho}{\partial\eta} - \beta\frac{\partial^2\rho}{\partial\eta^2} = 0. \tag{2.1}$$

The boundary conditions corresponding to the problem of Patnaik *et al.* (1976) are then

$$\rho \to \rho_0 \mp \tfrac{1}{2}\Delta\rho_0 \quad \text{for} \quad \eta/\delta \to \pm\infty.$$

We test a similarity solution

$$(\rho - \rho_0)/(\Delta\rho_0) = G(\xi), \tag{2.2}$$

where we take

$$\xi = \eta/\delta(t) \quad \text{and} \quad \delta(t) = \frac{\Delta\rho_0}{2(\partial\rho/\partial\eta)_{0,t}},$$

which implies that $G'(0) = -\frac{1}{2}$. Substitution of (2.2) into (2.1) leads to

$$\beta G'' + (\delta\delta' + \gamma\delta^2)\,\xi G' = 0. \tag{2.3}$$

This is an ordinary differential equation

$$G'' + K\xi G' = 0 \tag{2.4}$$

for G, provided that δ^2 obeys the ordinary differential equation

$$(\delta^2)' + 2\gamma\delta^2 - 2K\beta = 0 \tag{2.5}$$

† This feature of the numerical solution may appear inconsistent with the fact that the two stagnation streamlines evidently do not intersect at right angles. (See e.g. Patnaik *et al.* 1976, figure 4.) In fact, in his stationary solutions for a stratified shear layer, Maslowe (1972) found cusps at the stagnation point. But, whatever the local peculiarities of the stagnation streamline geometry, they are simply the kinematic result of the presence of local vorticity. The assumed local vorticity distribution, essentially a vortex sheet along a direction approaching that of one of the streamlines, cannot modify the local advective properties of the velocity field, an irrotational strain due to a remote vorticity distribution. Conversely, the evidence in Patnaik *et al.* for simple strain in this region is abundant. It includes the fact that the temperature braid is always straight (as is the stagnation streamline bearing the vorticity) and always has uniform thickness over a length $\gg$ the thickness.

for any constant K. The solution of (2.4) which meets the condition

$$G \to \mp \tfrac{1}{2} \quad \text{as} \quad \xi \to \pm\infty$$

is
$$G = -\tfrac{1}{2}\operatorname{erf}(\tfrac{1}{2}K^{\frac{1}{2}}\xi); \tag{2.6}$$

and the value of K implied by our definition of δ (as the half-thickness of the density profile) is $\frac{1}{2}\pi$. Thus, our approximation to the density profile of the braid is the error function

$$\rho = \rho_0 - \tfrac{1}{2}\Delta\rho_0 \operatorname{erf}(\tfrac{1}{2}\pi^{\frac{1}{2}}\delta). \tag{2.7}$$

δ is given by

$$\delta^2(t) = \delta^2(t_0)\exp\left[-\int_{t_0}^{t} 2\gamma(t')\,dt'\right] + \pi\beta\int_{t_0}^{t}\exp\left[-\int_{t'}^{t} 2\gamma(t'')\,dt''\right]dt'. \tag{2.8}$$

We saw in Patnaik *et al.* that γ is nearly independent of time during the last half of the period of vigorous wave growth. If γ remains constant for a sufficiently long time, the second term of (2.8) becomes dominant, and the braid thickness approaches the asymptotic value

$$\delta(\infty) = (\pi\beta/2\gamma(\infty))^{\frac{1}{2}}. \tag{2.9}$$

(Remember that β is the diffusivity for density, either thermal diffusivity or, say, salt diffusivity.)

When the Reynolds number is high (say, $U\delta/\nu \geqslant 100$), and the initial dimensionless layer thickness is not too small (say, $\alpha \equiv 2\pi\delta/\lambda \geqslant 0{\cdot}1$), the braid thickness will approach its asymptotic value from above. In many of the sample calculations made, the time to attain the asymptotic thickness was very close to the roll-up time of the wave.

2.2. *Similarity solution for the vorticity*

The vorticity equation derived from the Boussinesq momentum equations (2.1), (2.2) is

$$\frac{\partial\Omega}{\partial t} + u\frac{\partial\Omega}{\partial x} + v\frac{\partial\Omega}{\partial y} = \nu\left(\frac{\partial^2\Omega}{\partial x^2} + \frac{\partial^2\Omega}{\partial y^2}\right) - \frac{g}{\rho_0}\frac{\partial\rho}{\partial x}.$$

We can write this in the s, η co-ordinate system, with the same boundary-layer approximations used to write (2.1), and by disregarding the rotation of the new co-ordinate system. The result is

$$\frac{\partial\Omega}{\partial t} - \gamma\eta\frac{\partial\Omega}{\partial\eta} - \nu\frac{\partial^2\Omega}{\partial\eta^2} = -\frac{g\sin\theta}{\rho}\frac{\partial\rho}{\partial\eta}. \tag{2.10}$$

Substituting our result for the density profile, we obtain

$$\frac{\partial\Omega}{\partial t} - \gamma\eta\frac{\partial\Omega}{\partial\eta} - \nu\frac{\partial^2\Omega}{\partial\eta^2} = -\frac{g^*\sin\theta}{2\delta}\exp(-\tfrac{1}{4}\pi\eta^2/\delta^2), \tag{2.11}$$

where $g^* \equiv (\Delta\rho_0/\rho_0)\,g$.

If we test a solution in the similarity form

$$\Omega(\eta, t) = \frac{S(t)}{\delta_u(t)}H(\xi_u), \tag{2.12}$$

where $\xi_u = \eta/\delta_u$, we are led first to

$$\left(\frac{S'}{\delta_u} - \frac{S\delta_u'}{\delta_u^2}\right) H - \left(\frac{S\delta_u'}{\delta_u^2} + \frac{\gamma S}{\delta_u}\right) \xi_u H' - \frac{\nu S}{\delta_u^3} H'' = \frac{g^* \sin\theta}{2\delta} \exp\left(-\tfrac{1}{4}\pi\xi^2\right).$$

A homogeneous solution, satisfying the boundary conditions $\Omega_H \to 0$ as $\eta \to \pm\infty$ and the integral condition

$$\int_{-\infty}^{\infty} -\Omega_H \, d\eta = S_H,$$

is given by
$$H_H = \tfrac{1}{2} \exp\left(-\tfrac{1}{4}\pi\xi u^2\right), \tag{2.13}$$

provided that
$$(\delta_u^2)' + 2\gamma\delta_u^2 - \pi\nu = 0, \tag{2.14}$$

and that
$$S_H' + \gamma S_H = 0. \tag{2.15}$$

The baroclinic contribution to braid vorticity takes a simple analytic form only if the coefficients of diffusion for density and vorticity are equal. In this special case ($\nu = \beta$), we find that δ and δ_u obey the same differential equation. If we assume them equal initially, they remain equal. In this special case the general solution of (2.11) takes the similarity form (2.12), with

$$H = \tfrac{1}{2} \exp\left(-\tfrac{1}{4}\pi\xi^2\right), \tag{2.16}$$

provided that
$$(\delta^2)' + 2\gamma\delta^2 - \pi\nu = 0, \tag{2.17}$$

and that
$$S' + \gamma S - g^* \sin\theta = 0. \tag{2.18}$$

The baroclinic contribution to the problem appears in the last term of the equation for S. Whereas S tends to zero with large time in homogeneous flow (since $\delta > 0$), there is a finite limit

$$S(\infty) = g^* \sin\theta_\infty / \gamma_\infty \tag{2.19}$$

in baroclinic flows.

2.3. *The evolution of the vorticity in the braid*

According to the similarity solution, the initial vorticity of the braid is steadily depleted by the differential convection due to the strain along the braid. However, additional vorticity is generated baroclinically as a result of the tilting of the braid. The total vorticity per unit length of the braid generated in this way is independent of braid thickness, but the maximum value of the vorticity (found at the centre-line $\eta = 0$) is inversely proportional to the braid thickness, and therefore increases with the Reynolds number. As the braid becomes thin, the maximum vorticity becomes large; and it is of interest to investigate the likelihood that a secondary shear instability on a small scale (and of rapid growth) takes place.

We do not know exactly how the stability of an inclined shear layer is related to that of a horizontal one; but we guess that it may depend upon the component of gravity normal to the layer, and upon density and velocity derivatives in that same direction. For our similarity solutions, the minimum Richardson number of the braid occurs where $\eta = 0$, and can be evaluated from (2.2) and (2.12). First we find

$$J_B = -\left[\frac{g}{\rho}\frac{\partial\rho}{\partial z}[\Omega^2(0,t)]^{-1}\right]_{\eta=0} = \frac{g^*}{S^2}\frac{\delta_u^2}{\delta}\cos\theta\frac{G'(0)}{H^2(0)}.$$

Assuming that $\delta_u = \delta$, and substituting

$$G'(0) = -\tfrac{1}{2}, \quad H(0) = \tfrac{1}{2},$$

we get

$$J_B = 2g^*\delta/S^2 \cos\theta. \tag{2.20}$$

For a compact though anticipatory estimate, we can assume that $\gamma(t)$ and $\theta(t)$ have reached asymptotically constant values, and indeed that $\delta(t)$ and $S(t)$ have reached the limits given by (2.9) and (2.19). Then J_B approaches the limit

$$J_B(\infty) = (2\pi\nu)^{\frac{1}{2}} (\sin\theta_\infty \tan\theta_\infty)^{-1} \gamma_\infty^{\frac{3}{2}}/g^*. \tag{2.21}$$

As is clear from either Patnaik *et al.* or from arguments presented below, J_B is thus of order $Fr/Re_\lambda^{\frac{1}{2}}$, where $Fr = U^2/\lambda g^*$.

Computations were carried out to ascertain whether in fact secondary shear instability is possible before the wave reaches maximum amplitude. The similarity solutions were used, together with strain rates γ and braid slope angles θ given as functions of time by the dynamical model discussed below, rather than by the numerical computations of Patnaik *et al.* Two values of the Reynolds number were used for the braid calculations, $U\lambda/\nu = 5 \times 10^3$ and 5×10^5. The quantities computed were the braid Richardson number J_B towards the end of the primary-wave growth, the preferred wavelength λ_2 for the secondary-wave instability in terms of the primary-wave length λ, and the time ratio τ^* of secondary-wave roll-up time $2\lambda_2/S$ to primary-wave roll-up time λ/U.

Since these quantities evolve over time, the secondary instability develops on a layer for which neither the total shear nor the thickness is stationary. The typical values of J_B, λ_2 and τ^* to which we refer are not final, but those reached before the primary wave is of maximum amplitude, an interval of time sufficient for the secondary wave to develop fully. J_B, λ_2 and τ^* decrease monotonically with time as the primary wave grows, so that values chosen in this way may tend to under-estimate somewhat the degree of secondary instability.

The results of the computations show that for the lower Reynolds number, secondary instability is barely possible and probably rather rare. The value of J_B never falls below 0·13, for which, according to Patnaik *et al.*, the wave amplitude is small; and the roll-up time $\tau^* = 2\lambda_2 U/\lambda S$ is never smaller than 0·4 and often approaches unity, implying that the weak instability, when it occurs, proceeds rather slowly. On the other hand, for the higher Reynolds number, secondary instability should be prevalent over a rather wide range of values of primary-wave parameters J_0 and α. Figure 2 shows contours of constant non-dimensional secondary roll-up time τ^* in the α, J_0 plane. The way these contours close for $\alpha > 0{\cdot}4$ was only coarsely estimated, because the dynamical model that provides γ and θ in these computations is not applicable to short waves. (See §4.2.) For the contours shown, $J_B < 0{\cdot}04$ and $\lambda_B < 0{\cdot}025\lambda$. Hence short waves must appear along the braids, and roll up into small billows, before the primary wave has reached maximum amplitude. This phenomenon, the flow of energy from one length scale directly to a much smaller length scale, is a striking consequence of baroclinicity at high Reynolds numbers in a purely two-dimensional flow.

In the oceans, according to Thorpe (1973), billows are found as a result of the shear instability of layers for which, typically, $Re_\lambda \simeq 2{\cdot}4 \times 10^4$. In the atmosphere,

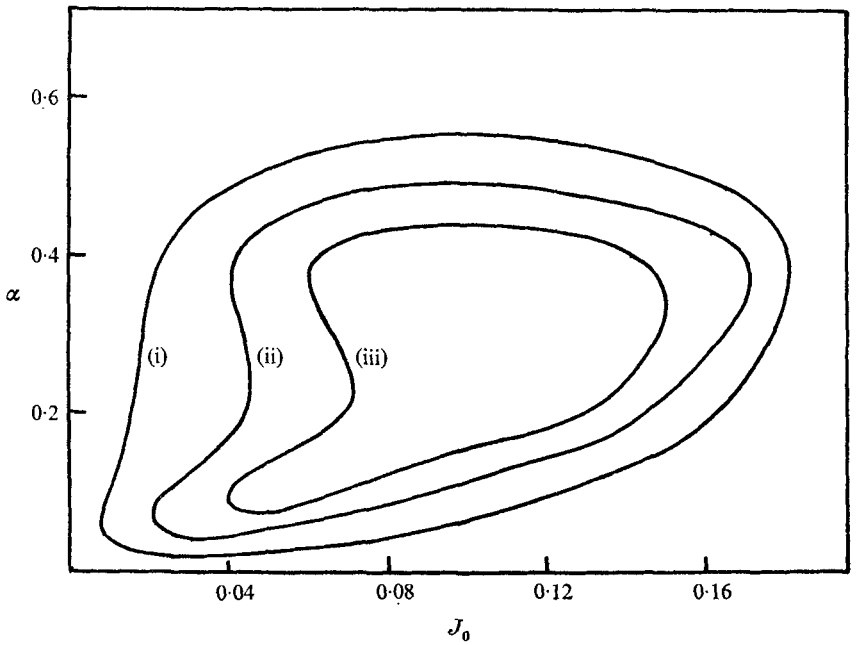

FIGURE 2. Criteria for secondary instability of the braids. $\tau^* = 2\lambda_2 U/\lambda S$, the ratio of roll-up time for secondary to that for primary instability. τ^*: (i) 0·1, (ii) 0·05, (iii) 0·04. Everywhere within the inner contour $\tau^* > 0{\cdot}03$. Everywhere within the outer contour $\lambda_2 \simeq 0{\cdot}02\lambda$ and $J_{0B} < 0{\cdot}04$. For all cases, $U\lambda/\nu = 500000$.

the same phenomenon occurs at values of Re_λ several orders of magnitude larger. Hence, we conclude that, in the atmosphere, secondary instability must be prevalent, and that in the oceans it is probably frequent also, though not for the smaller shear layers.

2.4. *Validity of the braid solutions*

The similarity solutions are consistent with the assumptions that led to the linearization of the convective terms. On the other hand, (2.18) states that the rate of decrease of the vorticity per unit length of the braid is the difference between a negative term (the rate at which vorticity is convected out of a section of the braid by the strain) and a positive (the local baroclinic rate of vorticity generation). The boundary condition used on the vorticity equation (namely, $\Omega \to 0$ as $\eta \to \pm\infty$) does not allow for the possibility that the streamlines that enter the braid from both sides might carry vorticity from regions outside this thin layer. That such recirculation of vorticity does not occur is not self-evident. In fact, it seems reasonable to believe the following *a priori*. (i) During the initial growth of the braids, all streamlines feeding them will carry vorticity. (ii) If the initial layer thickness is relatively large compared with the wavelength (α large), or if the Reynolds number is sufficiently low, streamlines entering the braid region will always involve rotational fluid. Suppose we exclude the initial period, low Reynolds number cases and short wavelengths. (That is, suppose we consider the finite amplitude development of waves reasonably similar to interfacial Kelvin–Helmholtz waves.) Even then it is possible to suspect that vorticity is

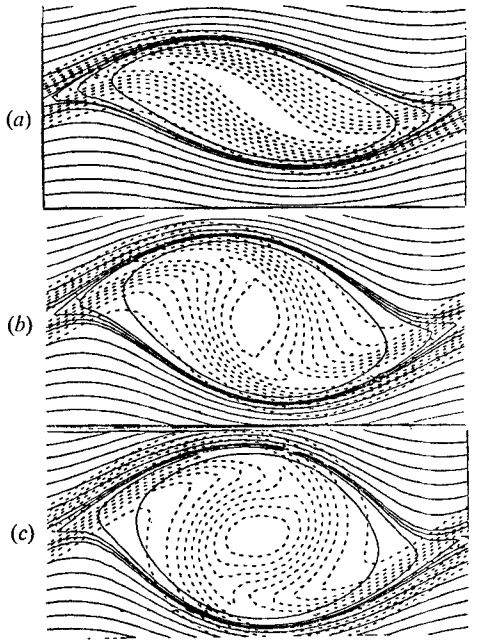

FIGURE 3. Vorticity and streamlines. Vorticity does not recirculate into the braids when $\alpha \leqslant 0{\cdot}2$. $\alpha = 0{\cdot}2$, $J_0 = 0{\cdot}03$, $U\delta/\nu = 25$, $Re_\lambda = 785$ ($Re_\delta = 25$). τ: (*a*) 0·5, (*b*) 0·75, (*c*) 1·0 (maximum amplitude).

recirculated into the braids, simply because it must diffuse at leisure throughout the closed streamlines of the flow, and half the braid streamlines are closed.

It is clear that, if vorticity is prevented from recirculating into the braids, it must be because the area enclosed by the stagnation streamlines (the area of recirculating flow) grows too rapidly for vorticity either to spread throughout this area, or to be advected along the full length of the dividing streamline towards the next stagnation point without entering the recirculating region. Accordingly, one would expect that, at about the time the wave stops growing, our braid solutions would begin to fail.

Inasmuch as the postulate that the vorticity originally advected along the braids penetrates the closed-streamline region and is trapped there is an essential component not only of the similarity solutions above, but also of the dynamic model which follows, it is worth inquiring further into its basis in fact. This can be done directly by plotting the streamlines and constant vorticity lines obtained from Patnaik *et al.* for a number of cases at various stages of the wave growth. This is done in Patnaik *et al.* (1976, figure 13); two more such plots are given in figures 3 and 4. They illustrate the inference that when $\alpha = 0{\cdot}2$, after a relatively short time, and even for $U\delta/\nu$ initially equal to 25, the streamlines entering the braid from either side involve only irrotational fluid, until a time exceeding that for maximum amplitude. On the other hand, when $\alpha = 0{\cdot}43$, the streamlines entering the braid carry some vorticity at all times.

Evidence of the validity of the similarity solutions for $\alpha \leqslant 0{\cdot}2$ is presented in figure 5. The figure compares the vorticity profiles $\Omega(\eta, t)$ given by the similarity

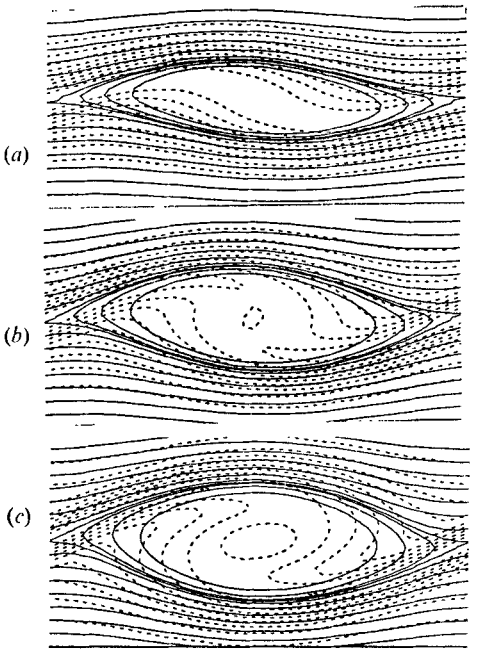

FIGURE 4. Vorticity and streamlines. Some vorticity recirculates at all times when $\alpha \geqslant 0{\cdot}43$. $\alpha = 0{\cdot}43$, $J_0 = 0{\cdot}07$, $U\delta/\nu = 50$, $Re_\lambda = 730$. τ: (*a*) 0·5, (*b*) 1·25, (*c*) 1·50 (maximum amplitude). ———, ψ contours; · · · · ·, Ω contours.

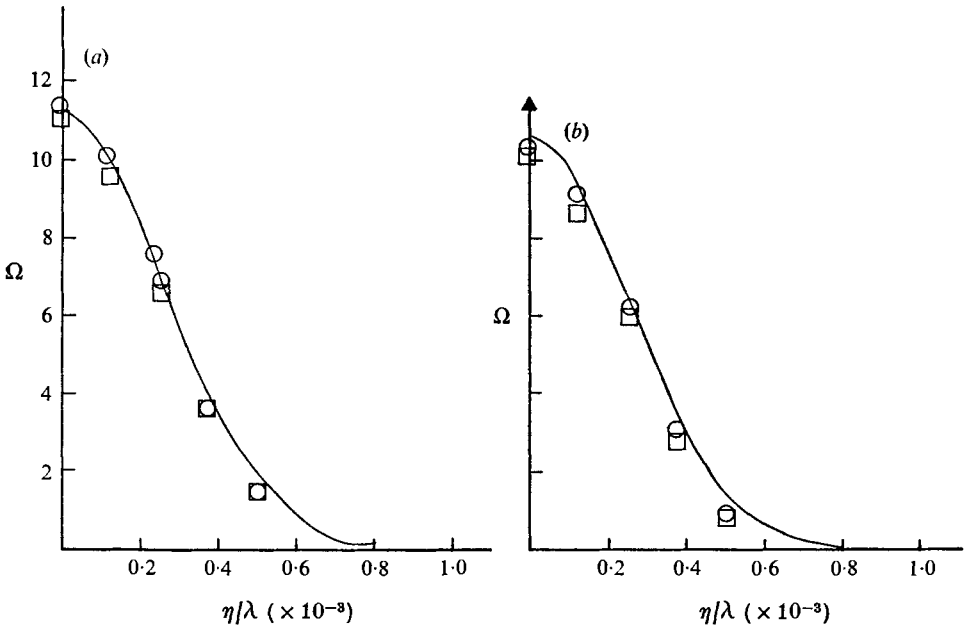

FIGURE 5. Comparison of the similarity solutions with the numerical solution of Patnaik *et al.* Vorticity structure of a braid near the stagnation point: $\alpha = 0{\cdot}2$, $J_0 = 0{\cdot}03$, $U\delta/\nu = 25$. τ: (*a*) 1·0, (*b*) 1·25. ○, $x/\lambda = 0$; □, $x/\lambda = \frac{1}{8}$.

solution with those given by the numerical solutions of Patnaik *et al.* in the vicinity of the stagnation point for a sample case. The case chosen is one in which the numerical 'diffraction fringes' discussed in Patnaik *et al.* are absent, by virtue of a sufficiently low Reynolds number.

3. The dynamics of growth to maximum amplitude for a given wave

The experimental evidence of Sato (1956), Freymuth (1966) and Browand (1966), the analysis of Kelly (1967) and the numerical solutions presented in Patnaik *et al.* all indicate both that an instability which originates at a given wavelength is capable of interacting with subharmonics, and that the growth of the subharmonics (waves that may be unstable in their own right) can be considerably enhanced by the presence of a primary wave of finite amplitude. This subject is of course of great importance. The growth of subharmonics enlarges the physical scale of the instability, and it is in general a fundamental part of the evolution of an unstable shear layer. For the present, we wish to restrict our account of nonlinear instability by ignoring these further (and in general later) steps in the systematic migration of vorticity into more distant and stronger centres. We offer the following word picture of the Kelvin–Helmholtz instability, and of the formation of billows which result.

During the early stages of growth of an infinitesimal periodic disturbance, it is easy to show that vorticity accumulates in regions which are periodically spaced. (See e.g. Batchelor 1967, p. 515.) This vorticity originates in other regions of the layer, which are consequently depleted. The accumulation of vorticity (in what will become the cores) causes a strain field, which is most intense half-way between the locations of the cores (the stagnation point regions). The strain is essentially proportional to the circulation around the region of vortex accumulation. This strain field causes the braids to be formed, thinned, stretched and inclined more or less along the direction of maximum strain. The ends of the stretched out braid wind up in the cores, and vorticity is thereby transferred from the braid into the cores. The increasing core vorticity induces a greater strain, a faster stretching rate (as well as a larger braid slope), and therefore an even more efficient vehicle for vorticity accumulation into the cores. Two further facts are required to describe the motion.

The total circulation around a loop, which encloses one wavelength of the growing perturbation, has the fixed value $\Gamma = -2U\lambda$, no matter what the stage of development of the billow or its degree of baroclinicity. This follows from the periodicity of the flow in the x direction and the limited range of y within which vorticity is found at any finite time.

Vorticity is generated baroclinically both in the braids and in the cores. The more the braids are tilted, the greater the baroclinic generation there. One may view the baroclinic generation or destruction in the cores as automatic compensation for that in the braids, since the total vorticity per wavelength remains constant.

At first, the braids lose more vorticity by advection into the cores than they gain by baroclinicity. Thus the core circulation increases. But the instability

is self-limiting when the rate at which vorticity can be drawn from the braids into the cores equals that at which fresh vorticity is generated within the braids.

In the uniform-density or barotropic case, the terminal state is one in which the vorticity of the braids is totally depleted.† In the baroclinic case, advective losses being eventually balanced by baroclinic generation, a fraction of the total vorticity remains in the braid. If the initial layer is gravitationally unstable, vorticity of sign opposite to that of the initial vorticity is produced baroclinically in the braids; the core vorticity increases without bound and exceeds $2U\lambda$ as soon as the braid vorticity changes sign. For this case, the instability is not self-limiting.

In general, the greater the fraction of the total circulation contributed by the vorticity within the stagnation streamlines (the cores), the larger the vertical excursion of these streamlines (i.e. the larger the amplitude of the waves).

The foregoing is meant to be a physical account of the main features of the instability. Tractable mathematical formulations of the process can now be found. It may be said that the most accurate make least specific use of the physical description, and that the simplest make a very literal use of it. Apart from a finite-difference or other numerical solution of the full equation, as in Patnaik *et al.*, an example of a method with controllable accuracy is one that makes use only of the fact that density and vorticity layers are thin if $\alpha \leqslant 0{\cdot}2$ and the Reynolds number is sufficiently large. We sketch such a method. According to what we have seen, except inside closed-streamline regions, where the details of the flow have not been thoroughly examined and where the spiralling braids may suffer compression and therefore thickening, it is possible to reformulate the stability problem by assigning vorticity and density contrast to a (advecting and distorting) curve, rather than to a finite area. If the finest details of the flow within the cores are not needed, this leads to a substantial simplification of the numerical task, and moreover to the possibility of a numerical evaluation at large Reynolds numbers. Let us fit the braids with a moving curvilinear co-ordinate system wherein, again, s is distance along the braid, and η distance normal to it. We assert (cf. §2) that an adequate approximation to the vorticity equation in the thin region occupied by the braid is

$$\frac{\partial \Omega}{\partial t}+\frac{\partial}{\partial S}(u\Omega)+\frac{\partial}{\partial \eta}(v\Omega) = \nu \frac{\partial^2 \Omega}{\partial \eta^2}+g/\rho_0 \frac{\partial \Theta}{\partial \eta}\sin\theta. \tag{3.1}$$

Equation (3.1) differs from (2.10) only in that variations of Ω along the braid are allowed, and the velocity is not assumed proportional to s. In particular, we retain the assumption that $\Omega = -\partial u/\partial \eta$. We integrate (3.1) with respect to η across the entire thickness of the braid, again making the assumption that vorticity and density gradients both vanish as $|\eta|$ increases to some fixed value η^*. We call

$$S = U^+ - U^- = -\int_{-\eta^*}^{+\eta^*} \Omega \, d\eta$$

† This description retains only what we consider the essential traits of the process. For a discussion of additional features of the motion apparent after the wave reaches maximum amplitude, see §4.1.

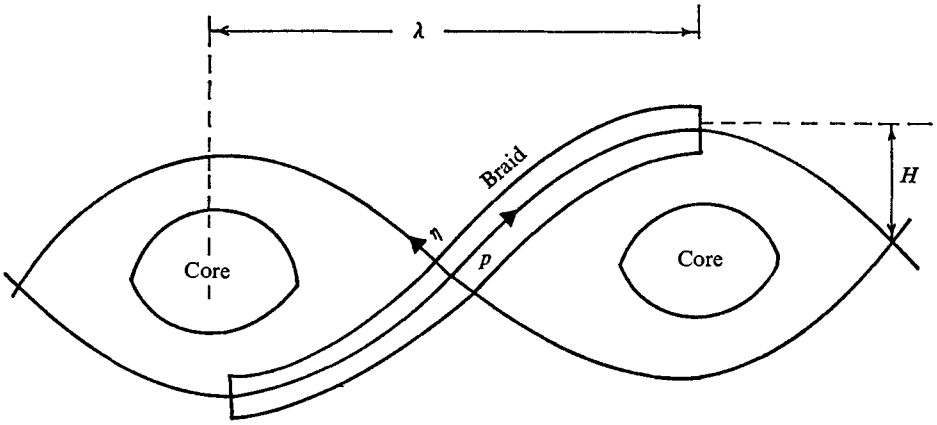

FIGURE 6. Co-ordinates for braid analysis.

the local shear across the braid, and find that S satisfies the hyperbolic equation

$$\frac{\partial S}{\partial \tau}+\overline{U}\frac{\partial S}{\partial s}=-S\frac{\partial \overline{U}}{\partial s}+g^*\sin\theta, \quad \text{where} \quad \overline{U}=\tfrac{1}{2}(u^+ + u^-). \tag{3.2}$$

It is possible to integrate (3.2), starting with a known velocity field given, say, by linear stability theory, and to recompute the velocity from the Biot–Savart Law at every time step after the shear has been advected (and generated) over a time step.

The integration of (3.2) can be carried out along the characteristics $ds/dt = \overline{U}$, and the co-ordinates of points of the sheet are advanced by finite-difference integrations of

$$\frac{dx}{dt}=\overline{U}[x(t),t]\cos\theta, \quad \frac{dy}{dt}=U[x(t),t]\sin\theta. \tag{3.3a,b}$$

A simpler scheme† and a more literal application of the physical description have been used. We first summarize the point of view of this model. We assign all the vorticity to two regions: (i) the cores centred at $x = \pm(\frac{1}{2}+n)\,\lambda$, around each of which the circulation is $\Gamma_c(t)$; (ii) thin braids that pass through the points $y = 0$, $x = \pm\eta\lambda$ $(n = 0, 1, 2\ldots)$, and that have a time-dependent configuration. A sketch of that configuration at a particular time is given in figure 6. As in the previous model, the vorticity and density braids being assumed very thin, their advection is computed by using the velocity on their centre-line. One keeps track of their location in space by a Lagrangian calculation of the trajectory of each part of the braid (in practice the determination of their abscissa suffices). One determines the rate of change of the shear across each point on the braid by computing local stretching and local slope (equation (3.2)).

The rate of transfer of vorticity from the braids to the cores (i.e. advective loss of braid vorticity) is now available and an overall budget of vorticity assigns

† The computational difficulties of tracing out even the barotropic roll-up of a vortex sheet are well documented, and extensions of this approach, to allow simulation of baroclinic effects in the Boussinesq approximation (Thomson & Meng 1975), show that accuracy can still be obtained only at considerable cost.

the correct value of circulation around the core without computing the detailed motion and baroclinic generation within the core.

Finally, we admittedly trade some accuracy for simplicity by postulating that, inasmuch as the velocity field that advects the braids is caused by vorticity at a distance, the precise configuration of this vorticity matters less than the total amount of circulation around it. We thus substitute for the braid-advecting velocity field one given by another flow with the same circulation around the cores at any time. Such a flow must, of course, (i) have the proper boundary conditions at infinity, (ii) give a cat's eye pattern with stagnation points located periodically in x, (iii) contain a parameter upon which depends the fraction of total vorticity contained within the cat's eyes.

For the braids, we shall make use of (3.2) and (3.3a). We now consider the temporal transfer of vorticity between the braids and the cores. We may call

$$\Gamma_B = \int_{-L}^{+L} S\,ds \tag{3.4}$$

the braid circulation. L denotes the (somewhat arbitrary) value of s at which the braid is imagined to end. The invariance of the total vorticity integral then requires that

$$\Gamma_B(t) + \Gamma_c(t) = \Gamma = 2U\lambda. \tag{3.5}$$

An ordinary differential equation for Γ_B or Γ_c is easily found by integrating (3.2) over s, from one end of the braid to the other. The result is

$$\frac{d\Gamma_c}{dt} = 2\left(\overline{U}_E - \frac{dL}{dt}\right) S_E - 2g^* H. \tag{3.6}$$

H is the elevation of the end of the braid above its centre; $\overline{U}_E$ is the braid centreline velocity at its ends; and S_E is the shear at the end of the braid. We shall solve (3.2) and (3.6) simultaneously as an initial-value problem, the specific procedure being to pick a number of points along the braid at time $t = 0$, assigning to them horizontal positions x and initial shears S_0. The latter are given by the formula

$$S_0 = \Gamma_{B\text{initial}}\,(1 - \epsilon \cos 2\pi x/\lambda)/\lambda, \tag{3.7}$$

suggested by linear theory. ϵ is an initial amplitude parameter; and the braid is taken to extend from $x = -\lambda/L$ to $x = +\lambda/L$. In a small time increment dt, the x's and S's are advanced by finite-difference integration of (3.3a), and of (3.2) in the form

$$\frac{dS}{dt} = -S\frac{\partial \overline{U}}{\partial s} + g^+ \sin\theta. \tag{3.8}$$

The time increment is automatically chosen so that one of the 'Lagrangian markers' arrives at the end of the braid at the end of each time step. A modified Euler predictor–corrector algorithm was used, with 41 initial points along a half-braid length.

One substitute velocity field that satisfies the conditions we placed on it is a set of periodic solutions to the inviscid steady vorticity equation presented by Stuart (1967). The stream function may be written

$$\psi = \frac{U}{k} \ln (\cosh ky + A \cos kx). \tag{3.9}$$

k is the x-wise wavenumber; and A is a parameter ranging from 0 to 1. When $A = 0$, we have a simple horizontal shear layer, $u = U \tanh ky$. When $A = 1$, we recover the classic solution for the flow produced by a row of equal line vortices located at $x = \pm \frac{1}{2}n\lambda$ ($n = 1, 2, 3, \ldots$). For all values of $A > 0$, the streamline pattern is of the expected cat's eye form. In particular, the streamline that outlines the cat's eye (the stagnation streamline) is given by

$$\cosh ky + A \cos kx = 1 + A.$$

The fraction of all vorticity contained within the cat's eyes, and considered the core vorticity, is related to A by

$$A = \tan^2(\tfrac{1}{4}\pi\, \Gamma_C/\Gamma). \tag{3.10}$$

The maximum vertical displacement of the stagnation streamline is

$$kH = \cosh^{-1}(1+2A) = \ln[1+2A+2(A+A^2)^{\frac{1}{2}}]. \tag{3.11}$$

Other properties of this streamline are discovered with seductive ease, a fact which may subtly have influenced our choice of this model, and the specific way we interpret it.

A material surface, which initially coincides with a stream surface, does not remain a stream surface during the course of an unsteady flow. But the computations of Patnaik *et al.* suggest that, except at the beginning of the growth, the braids always lie close to the stagnation streamline. So, in the model, the inclination and shape of the braids, and the stretching of the fluid therein, are assumed given by the properties found on the stagnation streamline in Stuart's solution. Thus, the advective field for the braid is the local velocity along the stagnation streamline

$$\overline{U} = 2U\left(\frac{A}{A+1}\right)^{\frac{1}{2}} \sin(\tfrac{1}{2}kx). \tag{3.12}$$

The rate of strain for the braid is

$$\gamma = \frac{\partial \overline{U}}{\partial s} = kU\left(\frac{A}{A+1}\right)^{\frac{1}{2}} \cos(\tfrac{1}{2}kx)\left(1 - \frac{A}{A+1}\cos(\tfrac{1}{2}kx)\right)^{\frac{1}{2}}. \tag{3.13}$$

The local inclination of the braid is

$$\sin\theta = \left(\frac{A}{A+1}\right)^{\frac{1}{2}} \cos(\tfrac{1}{2}kx). \tag{3.14}$$

An *a priori* idea of the errors involved in using Stuart's solution to advect the vorticity instead of the actual velocity field may be gained by comparing $\overline{U}$ from (3.12) with the velocity along the braid according to Patnaik *et al.*, on two bases: (i) equal values of Γ_C/Γ (i.e. $(\Gamma - \Gamma_B)/\Gamma$ for computations in Patnaik *et al.* and the circulation around the cat's eye for Stuart's solutions), and (ii) equal values of H/λ. (The definition of H is the same in the two types of computation.) This comparison (figure 7) indicates that, when Γ_C/Γ is the same, the values of velocity along the braid, and of the strain rate γ, are somewhat smaller in Stuart's solution than in the numerical. It also indicates that a greater value of Γ_c/Γ is required in Stuart's model than in the numerical solution

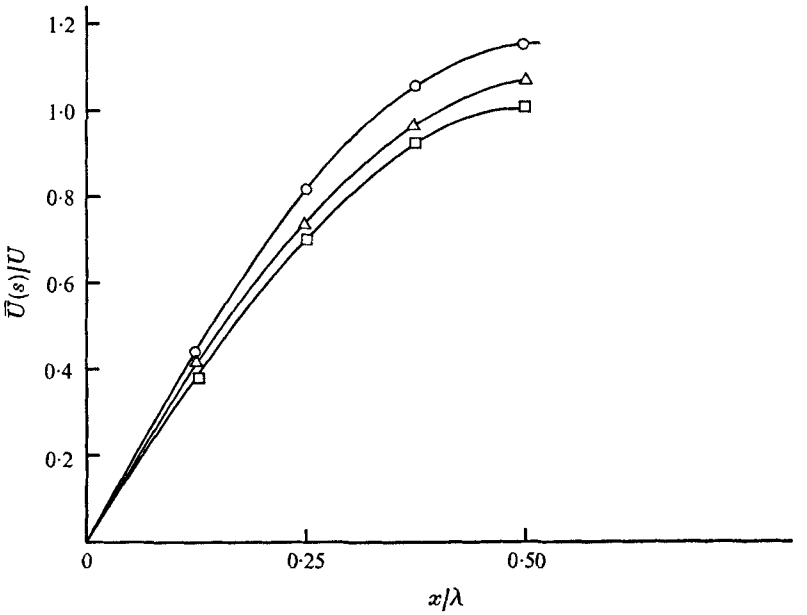

FIGURE 7. Comparison of the advective properties of Stuart's solution with those of the actual field (Patnaik *et al.*, numerical computation). △, numerical solution, $H/\lambda = 0{\cdot}21$, $\Gamma_c/\Gamma = 0{\cdot}67$; ○, Stuart solution, $H/\lambda = 0{\cdot}21$; □, Stuart solution $\Gamma_c/\Gamma = 0{\cdot}67$.

to achieve the same wave amplitude. Thus, we should expect use of Stuart's velocity field to underestimate both the growth rate and the maximum amplitude of the wave.

The integration of (3.3*a*) and (3.8) proceeded as follows. The 41 Lagrangian markers are given initial x values in a quasi-arbitrary way, designed to yield an optimal coverage of the entire length of the braid at all times. A small initial value of Γ_C/Γ or of H/λ is picked. Then the parameter A is evaluated, from (3.10) or (3.11), and initial values of $\overline{U}$, $\partial\overline{U}/\partial s$ and θ are calculated for each marker, from (3.12)–(3.14). The *initial* Γ_B and the *initial* S for each marker are calculated from (3.4) and (3.7), with $\epsilon = 0{\cdot}075$ in the latter.

After advancing x and S through a time step dt, for each marker, we recompute Γ_B from the quadrature (3.4), using $ds = dx \sec\theta$ and taking the limits to be $x = \pm\frac{1}{2}\lambda$. From this Γ_B a new value of A is found, the procedure for advancing the markers and their S values is repeated, and so on. The calculation stops automatically when the last marker reaches the end of the braid. By this time the asymptotic limit of A, and hence of H/λ and Γ_C/Γ, is easy to estimate by eye.

It should be pointed out that the dynamics invoked in this procedure assign no essential role to viscosity, so that the nonlinear instability mechanism is inviscid as long as the model is applicable. It is a simple matter to couple these computations with the similarity solutions presented earlier, and so to obtain the braid structure near the stagnation point as a function of time. This is how figure 2 was obtained. It is only at this stage that viscosity and thermal conductivity play a role.

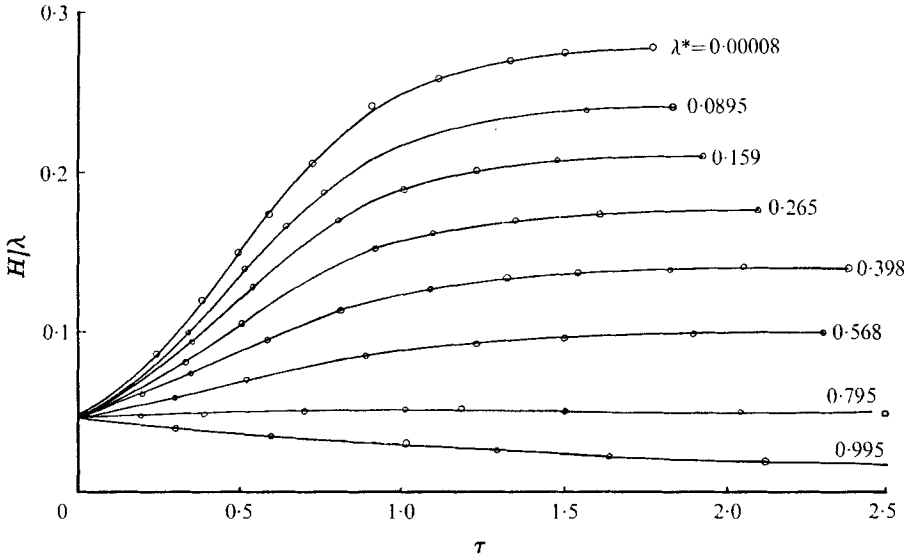

FIGURE 8. The amplitude of the wave as a function of time for waves of varying baroclinicity. Model predictions. $\tau = Ut/\lambda$.

4. The predictions of the model

The solutions provided by the model are dependent on two parameters

$$\lambda^* = g^*/2kU^2$$

(or equivalently the Froude number $U^2/g^*\lambda$), which is a measure of (i) the wave baroclinicity, and (ii) the assumed initial amplitude H_0/λ. Since the theory pertains to long enough waves, the parameter $\alpha = k\delta$ does not appear.

Sample histories of the amplitude as a function of time are given in graphical form in figure 8, for a comprehensive range of values of λ^* and an arbitrary initial amplitude. The limiting (homogeneous) case yields a maximum amplitude $H/\lambda \simeq 0{\cdot}280$. According to the model, if the wavenumber is such that $\lambda^* > 1{\cdot}0$, the wave never acquires a finite amplitude. This should be interpreted as follows. Even if the vorticity of the original layer is imagined concentrated in braids, the baroclinic generation in waves for which $k < g^*/2U^2$ exceeds, at all braid slopes, the rate of vorticity advection out of the braids and into the cores. Thus, baroclinic generation of vorticity of opposite sign within the cores more than makes up for vorticity gain from the braids, and no finite growth is possible. Linear interfacial theory (cf. Lamb, article 232) also yields, in the Boussinesq limit, $k = g^*/2U^2$, for the longest *infinitesimal* wave that can initially grow at all. Since the assumption underlying our model (no vorticity recirculation in the braids) depends on energetic growth, it is certainly inconsistent to use it to compute marginal growth cases involving excessively low values of Froude numbers. Thus, even for long wavelengths, it is not clear why the neutral condition according to linear theory (interfacial or diffusive) should agree with the criterion for zero growth calculated above. In fact, whenever our solutions predict slow growth (large values of λ^*), they probably overestimate both the growth rate and the maximum amplitude.

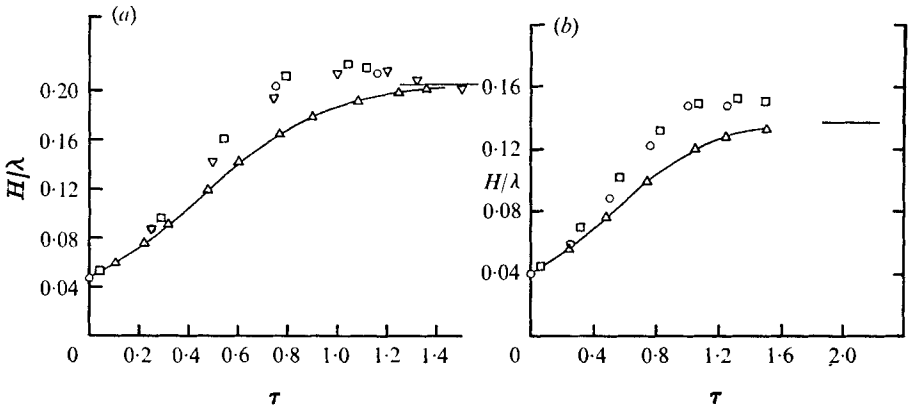

FIGURE 9. Comparison of model and numerical solutions when there is almost no vorticity recirculation. $\tau = Ut/\lambda$. $\alpha = 0{\cdot}2$. (*a*) $J_0 = 0{\cdot}03$, $\lambda^* = 0{\cdot}177$. (*b*) $J_0 = 0{\cdot}07$, $\lambda^* = 0{\cdot}412$. △, the model. Patnaik *et al.*: □, $U\lambda/\nu = 3142$; ○, $U\lambda/\nu = 1571$; ▽, $U\lambda/\nu = 785$.

The predictions of the model are compared with the numerical solutions of Patnaik *et al.* for two cases to which it should apply, and for two cases to which it should not.

4.1. *Long waves*

In figures 9(*a*), (*b*), the non-dimensional wavenumber $\alpha = k\delta = 0{\cdot}2$, and according to the Patnaik *et al.* computations there is no vorticity recirculation in the braids. One of the cases, figure 9(*a*), consists of three examples chosen from Patnaik *et al.* with essentially identical (relatively high) Froude numbers, but different Reynolds numbers. The growth of wave amplitude in time is compared with model predictions. The other case, figure 9(*b*), involves two examples of a lower Froude number.

It is seen from figures 9(*a*), (*b*) that, whenever vorticity does not recirculate in the braid, the effect of viscosity on the growth of the wave is small, according to the Patnaik *et al.* numerical solutions. This is true even for surprisingly low values of the Reynolds number. Such a result supports the treatment of the braid as a sheet. The model shows growth of wave amplitude slower than that of the numerical solutions. As we have seen, this is an expected consequence of using Stuart's velocity field to advect vorticity. The numerical solutions indicate, in addition, that the wave amplitude relaxes beyond the point of maximum amplitude. Examination of the plots of vorticity contours and of the streamlines for these cases show that the relaxation is due to two causes: (i) an apparent slight overshoot which, according to the numerical computations, is associated with a rotation of the core vorticity distribution; and (ii) the eventual entrainment of some core vorticity back into the braids, and its diffusion outside the closed-streamline regions, the instability having spent itself. We remarked earlier that the model is unable to describe this process. We should add that, in a real flow (i.e. one for which spacewise periodicity at fixed wavelength is not imposed), the growth of subharmonics, which proceeds at precisely that stage, generally overtakes the relaxation. The exception to this comes, in the case of stably

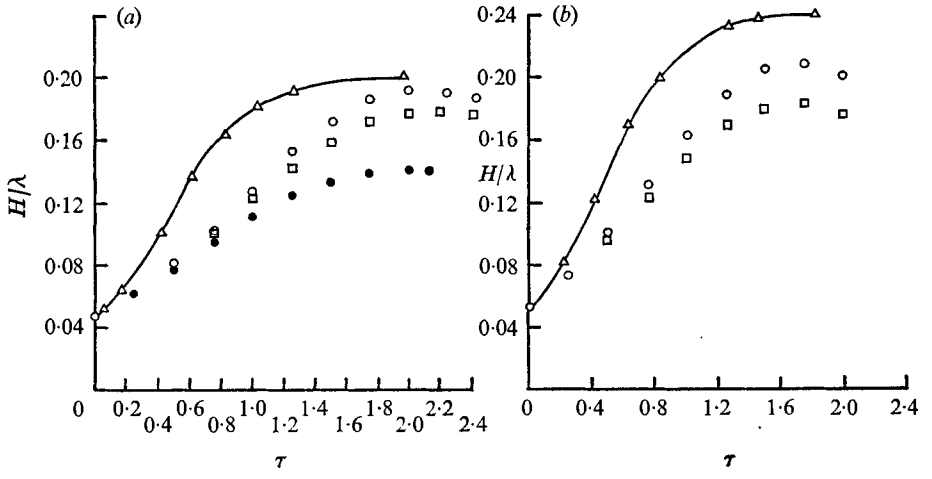

FIGURE 10. Comparison of model with numerical solutions when there is substantial vorticity recirculation. $\tau = Ut/\lambda$. $\alpha = 0{\cdot}43$. △, the model. (*a*) $J_0 = 0{\cdot}07$, $\lambda^* = 0{\cdot}192$. $U\lambda/\nu$, Patnaik *et al.*: ○, 2920; □, 1460; ●, 730. (*b*) $J_0 = 0{\cdot}03$, $\lambda^* = 0{\cdot}082$. $U\lambda/\nu$, Patnaik *et al.*: ○, 1460; □, 730.

stratified flow, after the last subharmonic growth event permitted by the given overall shear and stratification. Thus, for times exceeding that needed to achieve maximum amplitude, neither our model nor the Patnaik *et al.* numerical simulations describe the state of affairs realistically.

4.2. *Wavelength for maximum initial growth rate*

The comparison for the case $\alpha = 0{\cdot}43$ is shown in figures 10(*a*), (*b*). Since some vorticity is here likely to recirculate in the braids for all Reynolds numbers and all Froude numbers according to the numerical solutions, we should expect the basic assumption of our model to lead to some error. Figure 10 shows that the model overestimates both growth rate and maximum amplitude. The error introduced by the use of Stuart's velocity field is of course also present, and masks somewhat the discrepancy between model predictions and numerical solutions. For significantly larger values of α, the model predictions, which ignore recirculation, are worthless. This would be a serious drawback of the model were it not for the likelihood that waves of length shorter than that for maximum initial growth rate play no essential role in the nonlinear evolution of a shear layer. (This subject will be discussed in a subsequent paper.) On the other hand, perturbation techniques may be suitable for the study of those waves that are only mildly unstable, and that reach only modest amplitudes.

4.3. *An analytic approximation to the nonlinear growth of a wave*

It is a result of our model computations that, for the more baroclinic waves, or for late times, the shear varies little along the braid. Figure 11 illustrates this result at a time corresponding to the middle of the growth period. If we consider S independent of x, and if in addition we introduce an approximation to Stuart's solution, we can achieve a very simple analytic representation of our model. The

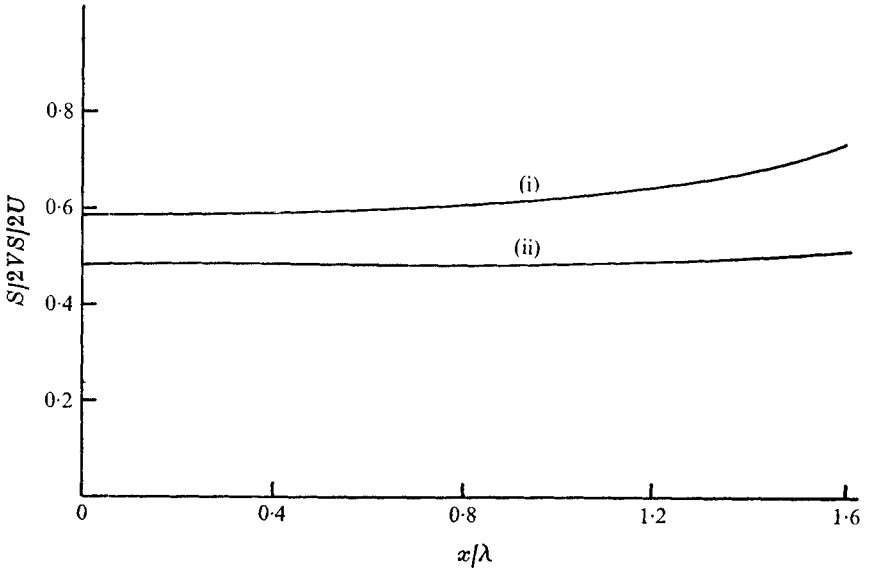

FIGURE 11. The shear across the braid as a function of x, for a strongly baroclinic case. Model predictions for $\lambda^* = 0{\cdot}412$. τ: (i) 0·78, (ii) 1·33.

results are less accurate than those we have presented, but the basic nonlinearity is displayed in a readily understandable form.

We retain (3.5), but neglect dL/dt as $\ll \bar{U}_E$:

$$d\Gamma_C/dt = 2\bar{U}_E S_E - 2g^* H. \tag{4.1}$$

According to (3.9)–(3.11), kH and $\bar{U}_E/U$ are monotonic functions of Γ_C/Γ that can, with a maximum error of 11%, be approximated by

$$\bar{U}_E/U \simeq kH \simeq \tfrac{1}{2}\pi G \quad \text{where} \quad G = \Gamma_C/\Gamma. \tag{4.2}$$

If we now use the assumption that S is independent of x, and take the braid length to be simply $2L = \lambda$, we get

$$S_E = \Gamma_B/\lambda = (\Gamma - \Gamma_C)/\lambda. \tag{4.3}$$

We can combine (4.1)–(4.3), to obtain

$$\frac{4\Gamma}{\lambda}\frac{dH}{dt} = \frac{d\Gamma_C}{dt} = \frac{\pi U}{\Gamma\lambda}\Gamma_C(\Gamma - \Gamma_C) - \frac{g^*\lambda}{2\Gamma}\Gamma_C. \tag{4.4}$$

The rate of growth of the wave amplitude is the difference between two terms: an advective term, the flux of vorticity into the cat's eye boundary, which is proportional to braid shear (i.e. $\sim \Gamma - \Gamma_C$) as well as to advective velocity (i.e. $\sim \Gamma_C$); and a baroclinic production term, proportional to braid slope (i.e. $\sim \Gamma_C$).

Non-dimensionally, (4.4) can be written

$$dG/dt = \omega_1 G - \omega_2 G^2, \tag{4.5}$$

where $\omega_1 = \frac{1}{2}Uk(1 - g^*/2kU^2)$, $\omega_2 = \frac{1}{2}Uk$. The solution is

$$\frac{H}{\lambda} = \tfrac{1}{4}G = \tfrac{1}{4}C\frac{\exp(\omega_1 t)}{1 + C(\omega_2/\omega_1)\exp(\omega_1 t)}.$$

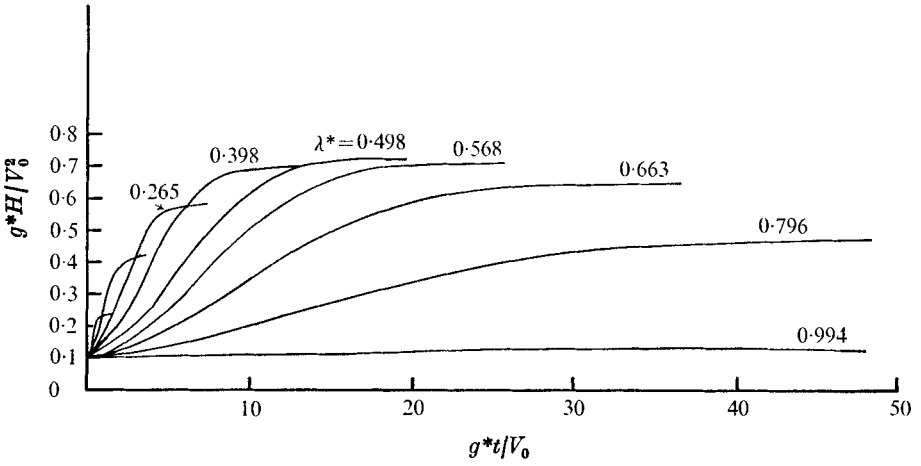

FIGURE 12. Wave amplitude against time in units that do not involve δ or λ. Model predictions.

C is an arbitrary constant, related to the initial amplitude H_0 by

$$C = \frac{4H_0/\lambda}{1-4H_0/\lambda}.$$

5. Comparison of waves growing independently in a given initial layer

It is of interest to compare the separate evolution of waves of different lengths on a non-dimensional basis, which involves only layer parameters. The amplitude parameter is then g^*H/U^2, and the non-dimensional time g^*t/U. This is shown in figure 12. We see that, while the shortest waves grow fastest, they achieve only modest maximum amplitudes, and that, since the longest waves do not grow at all, there is a preferred wavelength for waves that grow relatively slowly but achieve the largest amplitude. The model computations yield

$$\lambda^* = g^*/2kU^2 = 0{\cdot}5, \quad g^*H/U^2 = 0{\cdot}727 \quad \text{and} \quad H/\lambda = 0{\cdot}116$$

for these largest waves for which $G \cong 0{\cdot}5$. The maximum amplitude is reached at a time g^*t/U, which depends on initial amplitude, but which is roughly 10. Figure 13 shows the maximum amplitude against λ^*.

6. Interactions

One should bear in mind that the physical process described by the model rules out the possibility of waves of different wavelengths achieving their computed amplitude side by side. Vorticity lumping excludes vorticity sharing; and the fixed amount of vorticity available ($2U$/unit length) must be exclusively claimed by one wavelength, if the wave is to reach its maximum possible height. Thus, in order to describe the evolution of a layer initially disturbed in a non-selective manner, it is necessary to consider the interaction of waves of different wavelengths, which compete for the same supply of vorticity.

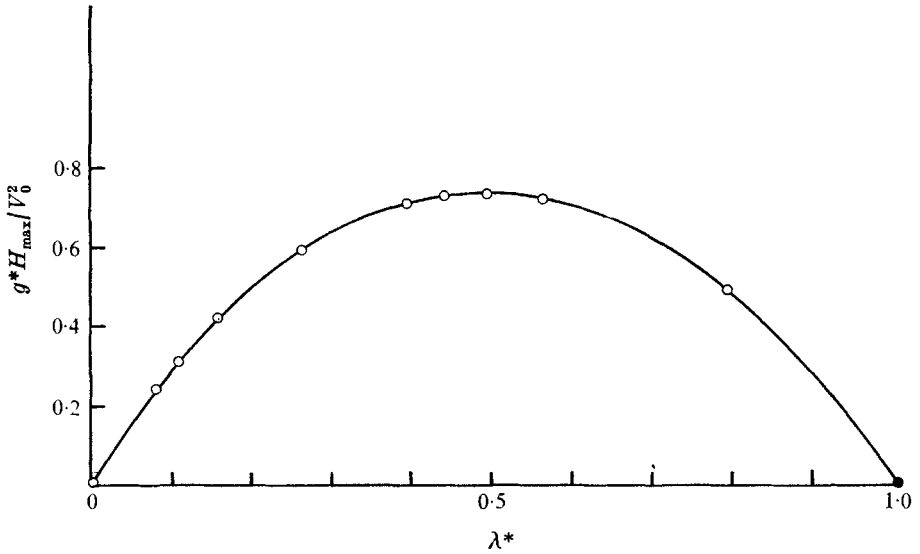

FIGURE 13. Maximum wave amplitude against baroclinicity. Model predictions.

Kelly (1967) studied the initial phase of a central aspect of this interaction, in an important and perceptive analysis of subharmonic growth. The same type of interaction will be examined as a nonlinear phenomenon in a subsequent article. Since the results of that work are required to describe the evolution of a simple shear layer in the laboratory or in natural flows, a comparison of predictions derived from our model and observations will be delayed until then. The relevance of Maslowe's (1972) stationary nonlinear diffusive wave solutions to the natural evolution of shear layers will also be discussed at that time.

7. Permanent mixing effects during the roll-up process

The important question of how much roll-up enhances permanent mixing can be answered partially by our model, if we confine our attention, as before, to the limited period ending when the wave reaches maximum amplitude. But the occurrence of secondary instabilities bears on the answer, so that gravitationally stable and gravitationally neutral mixing layers may behave quite differently in this regard, even during this initial period.

Let us assume first that there is no secondary instability. The constant density plots found in Patnaik *et al.*, and the numerical simulations of the roll-up of a vortex sheet modelled by a collection of discrete vortices, suggest strongly that it is primarily along the braids that positive strain occurs. The wound-up layer in the core, on the whole, suffers negative strain or compression. While most of the molecular mixing must eventually take place in the cores, it seems certain that the necessary development of small scales within that region requires a longer time than that available for roll-up. For instance, Brown & Roskho (1971), in their investigation of a turbulent free shear layer between gases of different

densities, found that "the variation in density at any point is of the same order as the density difference between the streams". This suggests that molecular mixing badly lags behind 'entrainment' (i.e. the circumscribing of fluid from both sides of the layer by closed streamlines). Thus, it seems reasonable to expect the mixing in a roll-up time to take place primarily in the braids.

Using our boundary-layer analysis of the braid again, we can estimate the total volume of fluid entrained into the mixing region $|\eta| \leqslant \delta$:

$$\text{volume mixed} \approx 2\lambda \int_0^T \left(\frac{d\delta}{dt} - v_\delta\right) dt.$$

From our braid model, we have

$$\frac{d\delta}{dt} = -\gamma\delta + \frac{\pi\beta}{2\delta} \quad \text{and} \quad v_\delta = -\gamma\delta.$$

γ is the strain rate along the braid, and $T = O(\lambda/U)$ is the roll-up time. Thus,

$$\text{volume mixed} \approx \pi\beta \int_0^T \frac{dt}{\delta(t)}.$$

Our model computations show that $\delta(t)$ reaches the asymptotic value

$$\delta(T) = \{\pi k/[2\gamma(T)]\}^{\frac{1}{2}},$$

which makes a convenient scale factor for the integral above. Finally, if we imagine that the volume of mixed fluid subsequently collapses back into a horizontal layer, the layer has a thickness

$$\frac{\Delta\,\text{mix}}{\lambda} = \left[\frac{2\pi\gamma^*(T)}{RePr}\right]^{\frac{1}{2}} \int_0^{\tau(T)} \frac{\delta(T)}{\delta(t)} d\tau, \quad \text{where} \quad \gamma^* = \lambda\gamma/U, \quad \tau = tU/\lambda.$$

The dimensionless integral varies from about 0·4 to 1·2, within the range of examples examined. These include typical values of the parameters α and λ^*. In most cases, the increase in mixed layer thickness during roll-up is small compared with billow height. The ratio is $\sim \frac{1}{4}$ for $Re_\lambda = 1000$, and decreases to $\frac{1}{100}$ for $Re_\lambda = 500\,000$.

In summary, it seems that, in the absence of secondary instability, roll-up is only a prelude to permanent mixing. On the other hand, in the stratified case, if the Reynolds number is high, (i) a secondary instability should be expected; (ii) the roll-up time for the secondary billows (with wave lengths likely to be small) is short, so that it is quite possible not only for these billows to entrain additional fluid, but also for the subharmonic growth of the small billows to contribute further to the mixing in the region of the braid while the primary wave is still growing. The qualitative effect of these phenomena, according to our model, is thus to enhance the mixing by the braid, as though the Reynolds number were lower.

This work was partly supported by the National Science Foundation under contract GA-35783. The authors are indebted to Dr P. C. Patnaik for a number of computations carried out at their request. They also benefited from very fruitful discussions with Professor F. Browand.

REFERENCES

BATCHELOR, G. K. 1967 *An Introduction to Fluid Dynamics.* Cambridge University Press.

BROWAND, F. K. 1966 An experimental investigation of the instability of an incompressible separated shear layer. *J. Fluid Mech.* **26**, 281–307.

BROWN, F. L. & ROSHKO, A. 1971 The effect of density difference on the turbulent mixing layer. *AGARD Conf. Proc. Turbulent Shear Flows.*

FREYMUTH, P. 1966 On transition in a separated boundary layer. *J. Fluid Mech.* **25**, 683–704.

KELLY, R. E. 1967 On the stability of an inviscid shear layer which is periodic in space and time. *J. Fluid Mech.* **27**, 657–689.

LAMB, H. 1932 *Hydrodynamics.* Dover.

MASLOWE, S. M. 1972 The generation of clear air turbulence by nonlinear waves. *Stud. Appl. Math.* **51**.

PATNAIK, P. C., SHERMAN, F. S. & CORCOS, G. M. 1976 A numerical simulation of Kelvin–Helmholtz waves of finite-amplitude. *J. Fluid Mech.* **73**, 215–240.

SATO, H. 1956 Experimental investigations of the transition of laminar separated layer. *J. Phys. Soc. Japan*, **11**, 702–709, 1128.

STUART, J. T. 1967 On finite-amplitude oscillations in laminar mixing layers. *J. Fluid Mech.* **29**, 417–440.

THOMSON, J. A. L. & MENG, J. C. S. 1975 Studies of free buoyant and sheer flows by the vortex-in-cell method. *Lecture Notes in Physics*, vol. 35. Springer.

THORPE, S. A. 1973 Turbulence in stratified fluid. *Boundary-Layer Met.* **5**, 95.